JACC Vol. 18, No. 7
December 1991:1794–803

Experimental Model of Chronic Global Left Ventricular Dysfunction Secondary to Left Coronary Microembolization

STEVEN J. LAVINE, MD, FACC, PETAR PRCEVSKI, DVM, A. CHRISTIAN HELD, MD, FACC, VICKI JOHNSON

Detroit, Michigan

A model of chronic left ventricular dysfunction characterized by left ventricular dilation, elevated filling pressures and histologic changes has been lacking. In this study the use of coronary microsphere embolization-induced ischemia was explored as a method of producing chronic left ventricular dysfunction. Acute ischemic left ventricular dysfunction was induced in 13 mongrel dogs with 50 μm plastic microspheres until the peak positive first derivative of left ventricular pressure (dP/dt) decreased by 25% and the left ventricular end-diastolic pressure increased to ≥12 mm Hg. After 8 weeks of observation, hemodynamic and echocardiographic variables were measured in each dog.

Acute left ventricular dysfunction resulted in a dilated left ventricle with systolic dysfunction (area ejection fraction 24 ± 6% vs. 57 ± 9% initially, $p < 0.01$) and elevated left ventricular filling pressures. Isovolumetric relaxation was prolonged and the peak rapid filling/atrial filling velocity and integral ratios were reduced.

Eight weeks after embolization, there was an increased left ventricular size (end-diastolic area 15.1 ± 2.1 cm^2 at 8 weeks vs. 13.5 ± 1.4 cm^2 early after microsphere injection, $p < 0.05$), unchanged end-systolic area, improved area ejection fraction and increased left ventricular mass. Left ventricular end-diastolic pressure increased and, despite continued abnormal relaxation, the peak rapid filling/atrial filling velocity and integral ratios increased to above baseline values, demonstrating a "restrictive" pattern. Gross and histologic examination revealed diffuse, patchy scarring associated with perivascular fibrosis.

Thus, coronary microsphere embolization resulted in a model of chronic moderate left ventricular systolic dysfunction and abnormal diastolic function characterized by a "restrictive" filling pattern.

(J Am Coll Cardiol 1991;18:1794–803)

A canine model of chronic left ventricular dysfunction characterized by a dilated left ventricle and elevated left ventricular filling pressures would provide an important experimental means for characterizing hemodynamic and neurohormonal alterations associated with progressive heart failure. To date, a variety of different experimental preparations have been utilized, including pressure loading, volume loading, venous obstruction, right heart failure, ischemia and the use of toxins (1). However, none of these techniques have been entirely successful in producing a canine model of chronic left ventricular dysfunction associated with left ventricular dilation and filling pressure elevation. Rapid right ventricular pacing was utilized to produce a reversible canine model of congestive heart failure (2,3), but it lacked histopathologic alterations. Although the rapid ventricular pacing model shares some of the hemodynamic and neurohormonal alterations seen in chronic congestive heart failure in humans, the lack of myocardial scarring characteristic of many patients with a failing left ventricle is an important limitation of the pacing model, especially with regard to the evaluation of diastolic function.

Recently we (4–6) explored the use of coronary embolization with small (50 μm) plastic microspheres as a means of producing acute low output congestive heart failure to study diastolic function in acute congestive heart failure. With this acute model, we have confirmed our previous clinical observations (7) that redistribution of diastolic filling to early in diastole occurs with severe left ventricular dysfunction and elevated mean pulmonary capillary pressures. Our experimental data (5) indicate that increased pericardial restraining forces mediate this diastolic filling redistribution. The ability to generalize these experimental findings to clinical chronic congestive heart failure is obviously limited because of the nature of this short-term model. However, the coronary microsphere model of low output congestive heart failure may be particularly well suited for the study of chronic disease because the histopathologic changes (patchy fibrosis throughout the myocardium) share some similarity to the histologic changes seen in patients with chronic congestive heart failure of various causes (8–10).

In this study, we report our use of 50 μm coronary microsphere embolization to produce a canine model of chronic left ventricular dysfunction with elevated left ventricular filling pressures. The systolic and diastolic functional

From the Division of Cardiology, Harper Hospital, Wayne State University, Detroit, Michigan.

Manuscript received December 13, 1991; revised manuscript received May 22, 1991, accepted June 7, 1991.

Address for reprints: Steven J. Lavine, MD, Division of Cardiology, Noninvasive Laboratory, Harper Hospital, 3990 John R, Detroit, Michigan 48201.

0735-1097/91/$3.50

responses to acute ischemic left ventricular dysfunction and to the left ventricular remodeling associated with chronic left ventricular dysfunction are described.

Methods

Experimental preparation. The animals used in this study were maintained in accordance with the guidelines of the Committee on Animal Studies at Wayne State University School of Medicine and those prepared by the Committee on Care and Use of Laboratory Animals of the Institute of Laboratory Animal Resources, National Research Council (DHEW Publication No. [NIH] 85-23, revised in 1985). Anesthesia was induced in 13 conditioned mongrel dogs (19 to 27 kg) with morphine sulfate (1.5 mg/kg) and acepromazine (1.1 mg/kg) injected intramuscularly followed in 15 min by 30 mg/kg of ketamine hydrochloride administered intravenously. Maintenance anesthesia was produced by intravenous morphine sulfate (1.5 mg/kg per h) and sodium pentobarbital (3 mg/kg per h). The dogs were intubated and artificially ventilated with a Harvard respirator using room air. Two 7F high fidelity pressure catheters (Millar Instruments) were introduced into the right carotid artery and, guided by fluoroscopy, one was advanced into the left ventricle and the other into the ascending aorta. A size 8 multipurpose Judkins coronary catheter was introduced through an arterial sheath (Cordis) into the right femoral artery and advanced into the left coronary ostium under fluoroscopic guidance; small bolus doses of a nonionic contrast medium were used to verify its position. A 7F thermodilution pulmonary artery flotation catheter was introduced through the right femoral vein and advanced to the pulmonary artery with fluoroscopic guidance. The proximal port was utilized to obtain mean right atrial pressure. Also, through the right femoral vein, a no. 5 bipolar pacing wire was advanced fluoroscopically to the high right atrium. After all the catheters were in place, heparin (3,000 U) was administered intravenously. Continuous electrocardiographic (ECG) recordings utilizing lead II were obtained. At held end-expiration, the ECG, left ventricular pressure and first derivative of left ventricular pressure (dP/dt), central aortic pressure and mean right atrial pressure were displayed on an eight-channel physiologic recorder (Gould) and recorded at paper speeds of 100 and 200 mm/s. Thermodilution cardiac output was measured in triplicate.

Echocardiography. Simultaneous two-dimensional echocardiograms were obtained from the parasternal short-axis view at the mid-papillary muscle level with use of a phased array ultrasonograph (Hewlett-Packard 77020-A or Aloka 880). From the parasternal short-axis views, cursor-derived M-mode recordings of the mitral valve and left ventricle were obtained together with phonocardiographic recordings of the heart sounds recorded at a rate of 100 mm/s on a strip chart recorder. Transesophageal four-chamber and apical long-axis images were obtained from a commercially available 5 MHz transesophageal probe (Hewlett-Packard or Aloka) placed in the dog's mid-esophagus. Transmitral pulsed Doppler recordings were obtained with the sample volume placed between the tips of the mitral leaflets in diastole and recorded on a strip chart recorder at 100 mm/s. The left atrium was examined for the presence of mitral regurgitation with use of pulsed Doppler echocardiography and color flow mapping. The extent of mitral regurgitation was semiquantified by determining the area of the maximal regurgitant color flow signal as a function of left atrial size in the apical four-chamber, apical long-axis and parasternal long-axis views. The final ratio was derived from the average of the three views with use of three consecutive beats. The preceding hemodynamic, echocardiographic and Doppler data were acquired at baseline and during various atrial pacing rates beginning at 10 beats above baseline and incremented at 5-beat intervals until merging of the transmitral pulsed Doppler rapid and atrial filling integrals occurred.

Coronary microsphere embolization. Ischemic left ventricular dysfunction was induced by left main coronary artery injection of (58 ± 2 μm in diameter) plastic microspheres (3M) (4.5). The microspheres were continuously agitated in a saline suspension and injected as a bolus of 2 to 4 ml (35,000 microspheres/ml). Injections were made every 5 to 10 min until the peak positive dP/dt decreased by ≥25% and the left ventricular end-diastolic pressure was ≥12 mm Hg. The average dose of coronary microspheres was 0.21 million microspheres (range: 0.14 to 0.32 million). Moderate left ventricular systolic dysfunction associated with moderate left ventricular filling pressure elevation was achieved in approximately 45 to 60 min. After 60 min of hemodynamic stability, echocardiographic, ECG, hemodynamic and cardiac output variables were obtained without atrial pacing and at an atrial pacing rate that matched one of the atrial pacing rates used before coronary microsphere embolization. Minor adjustments were made in the pacing catheter's position to ensure that the PR interval was the same as that acquired before embolization. The right carotid and femoral arteries were repaired with good distal flows and the right femoral vein was ligated. The skin was sutured and anesthesia was partially reversed with 0.4 mg of nalaxone intravenously. Three dogs died of severe pulmonary edema within 48 h. The 10 surviving dogs were transferred to the veterinary hospital for convalescence.

Follow-up. All 10 dogs were observed for 8 weeks and followed up with daily weight measurement and weekly parasternal short-axis echocardiograms obtained with the dogs lying quietly on their right side. No further complications were noted in this group. Furosemide (20 mg intravenously) was utilized for the first 48 h to alleviate pulmonary congestion, as assessed by lung examination and assessment of the dog's respiratory rate and depth of respiration. Dyspnea did not appear to be a significant problem after 48 h.

Experimental protocol 8 weeks after embolization. Eight weeks, after coronary artery microembolization, each dog was returned to the experimental laboratory. Anesthesia was induced with the induction and maintenance anesthesia

JACC Vol. 18, No. 7
December 1991:1794–803

protocol previously described. High fidelity (7F) pressure catheters (Millar) were placed into the left ventricle and ascending aorta through the left femoral and left carotid arteries. A 7F thermodilution pulmonary artery flotation catheter and a no. 5 bipolar pacing wire were introduced into the pulmonary artery, as previously described. The position of the pacing catheter was adjusted to ensure that the same PR interval was obtained. After all the catheters were in place, heparin (3,000 U) was administered intravenously. Continuous ECG recordings utilizing lead II were obtained. At held end-expiration, hemodynamic, echocardiographic and Doppler variables were recorded without pacing and at the same atrial pacing rate used during acute ischemic left ventricular dysfunction. In each dog, the heart was then fibrillated with 1 cc/kg of potassium chloride. The heart with intact atria was excised and weighed on an electronic balance.

Hemodynamic variables. Left ventricular systolic, minimal and end-diastolic pressures, peak positive and peak negative dP/dt, mean right atrial pressure, mean arterial pressure and cardiac output (stroke volume) were obtained from the hemodynamic tracings at baseline after the production of acute left ventricular dysfunction and at 8 weeks after embolization at the same atrially paced rate. The rapid filling wave on the left ventricular pressure tracing, as defined by the pressure increment between the minimal left ventricular pressure and the pressure plateau before the A wave, was obtained from three consecutive beats and averaged. The time constant of left ventricular pressure decline, a measure of left ventricular diastolic relaxation, was calculated with use of a monoexponential fit of left ventricular pressure with time assuming a zero asymptote (11). Hemodynamic data demonstrated excellent fits with the exponential relation ($r > 0.99$). All hemodynamic measurements were calculated as an average of three consecutive beats or determinations.

Isovolumetric relaxation period and left ventricular wall thickness. From the mitral valve echogram and phonocardiographic recordings (at 100 mm/s paper speed), we obtained the intervals from the Q wave to the opening of the mitral valve and from the Q wave to the aortic component (first high frequency component) of the second heart sound (total left ventricular systolic time). The isovolumetric relaxation period was defined as the interval from the Q wave to the opening of the mitral valve minus the total left ventricular systolic time. From the M-mode echocardiographic recordings of the left ventricle, septal and posterior wall thickness were obtained with use of conventional measurement techniques (12). Left ventricular mass was calculated by using the M-mode technique of Devereaux and Reichek (13). Each of the intervals was obtained from the three consecutive cycles and averaged at baseline, during acute left ventricular dysfunction and at 3 weeks.

Transmitral pulsed Doppler recordings. Because transmitral spectral tracings were obtained from the transesophageal window, they were negatively directed because the direction of flow was away from the transducer. Tracings were digitized (10-ms intervals) with use of a hand-held digitizer with a graphics tablet and the Doppler analysis package of the Quantic 1200 (Bruce Franklin). From the average of measurements taken from three consecutive tracings, we obtained the peak rapid filling and atrial filling velocities. The rapid filling period was defined as the interval from the onset of mitral flow to the end of rapid filling, the atrial filling period as the interval from the onset of atrial filling to the end of mitral flow and the diastolic filling period as the interval from the onset to the end of transmitral flow. In this study a wall filter (0.1 m/s) was used for each dog at baseline, during acute left ventricular dysfunction and at 8 weeks after embolization. Because the wall filter in this instrument produced a velocity cutoff, we extrapolated the spectral tracings perpendicularly to the baseline. All timing measurements were taken from the baseline. Perpendicular extrapolation to the baseline resulted in high reproducibility (mean difference 6 ± 2 ms) of timing interval determination. Linear extrapolation to the baseline may alter the timing interval, but in all dogs and in all conditions the mean difference was <10 ms. The area beneath the spectral tracing was determined for the rapid, atrial and diastolic filling periods. Both rapid and atrial filling areas were divided by the diastolic filling area to generate a rapid filling and atrial filling fraction.

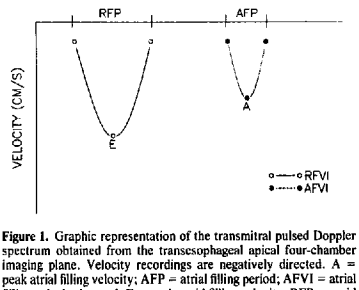

Figure 1. Graphic representation of the transmitral pulsed Doppler spectrum obtained from the transesophageal apical four-chamber imaging plane. Velocity recordings are negatively directed. A = peak atrial filling velocity; AFP = atrial filling period; AFVI = atrial filling velocity integral; E = peak rapid filling velocity; RFP = rapid filling period; RFVI = rapid filling velocity integral.

Echocardiographic analysis of left and right ventricular areas. Three consecutive cardiac cycles from each stage (atrially paced) were analyzed by a single operator using an off-line commercially available analysis system (Quantic 1200). Left ventricular short-axis area was digitized on a frame by frame basis from videotape from three consecutive cardiac cycles. For each cardiac cycle, an area versus time curve was constructed. End-diastolic area was determined as the frame with the largest digitized area and end-systolic area as the frame with the smallest digitized area. Stroke area was calculated as the End-diastolic area − End-systolic

area and area ejection fraction as the Stroke area/End-diastolic area.

Left ventricular wall motion was assessed by two observers who had no knowledge of other data using a semiquantitative visual analysis of the parasternal short-axis, apical four-chamber and apical long-axis views. The apical views were divided into five segments. The parasternal short-axis view was also divided into five segments (anterior, septal, lateral, inferior and posterior walls). Each segment in each view for each condition was scored on a scale of 1 to 5 with 1 = normal wall motion and 5 = dyskinesia. The observers agreed on 98% of segments and all disagreements were resolved by consensus. Global dysfunction was defined as an increase in score for each segment by at least 2 over baseline and a maximal difference between segments of ≤1 semiquantitative unit for a given condition (acute left ventricular dysfunction or 8 weeks after embolization).

Right ventricular end-diastolic (at the R wave) and end-systolic areas were determined from the transesophageal apical four-chamber view. An area ejection fraction was calculated, as described previously. The filling fractions at one third and one half of diastole (two indexes characterizing the extent and time course of diastolic filling [5]) were calculated from this frame by frame analysis. The filling fraction (FF) at one third and one half of diastole (D) was calculated as:

$$\text{FF at 1/3 D} = \text{1/3 DA} - \text{ESA/Stroke area}$$

$$\text{FF at 1/2 D} = \text{1/2 DA} - \text{ESA/Stroke area,}$$

where 1/3 DA = digitized left ventricular area at one-third diastole, 1/2 DA = digitized left ventricular area at one-half diastole and ESA = end-systolic area. If the time of one-third or one-half diastole fell between frames, linear interpolation between the two closest frames was used to calculate the appropriate filling fraction. The filling fraction at one-third and one-half of diastole represents the percent of left ventricular short-axis area expansion at one-third or one-half of total diastole. Total diastole necessarily includes the isovolumetric relaxation period because the midpapillary muscle level short-axis view does not include visualization of mitral valve motion. All echocardiographic variables were calculated as the average of three consecutive cycles.

Left ventricular pressure-volume relations. Simultaneous left ventricular pressures and echocardiographic left ventricular short-axis areas from end-diastole to end-systole were plotted every 33 ms for the baseline state, acute left ventricular dysfunction and 8 weeks after embolization. Simultaneous left ventricular pressures and echocardiographic short-axis areas from the minimal left ventricular pressure to the peak of the A wave were fitted ($r > 0.98$) to the following exponential equation (14,15): $P = be^{kA}$, where P = left ventricular diastolic pressure, b = a constant, e = base of the natural logarithm, k = chamber stiffness constant and A = left ventricular short-axis area. The chamber stiffness constant (k) was calculated as the slope of the linear relation between the natural logarithm of the left ventricular pressure and short-axis area: $\ln P = kA + \ln b$. A linear least squares method was used to find the slope of the best fitting line.

Intraobserver variability for left ventricular cavity area for a given video frame was determined by analysis of 25 randomly chosen frames from seven previously studied dogs. Each frame was analyzed twice at least 2 weeks apart. The average difference between measurements for a given frame was 0.25 cm^2 (or 1.6 ± 1.2% of the left ventricular area).

Left ventricular geometry and wall stress. From the transesophageal apical long-axis view of the left ventricle, the end-diastolic (at the R wave) and end-systolic (smallest area) areas were determined. The long axis of the left ventricle at end-diastole and end-systole was determined as the linear distance from the echocardiographic apex of the left ventricle to the insertion of the anterior mitral leaflet. Although the apical four-chamber view in humans tends to foreshorten the left ventricle (especially with transesophageal imaging), in dogs this view tends to provide a closer approximation to the long axis of the left ventricle. The minor axis of the left ventricle for end-diastole and end-systole can be calculated from the apical four-chamber view (A4C) with use of a variation of the area-length formula (16):

$$\text{Minor axis (A4C)} = 4 \times \text{A4C area}/3.14 \times \text{Long axis.}$$

A second minor axis can be calculated from the end-diastolic and end-systolic short axis (SAX) areas with the following formula:

$$\text{Minor axis (SAX)} = 2\,(\text{short axis area}/3.14)^{1/2}.$$

For a prolate ellipse, the ratio of the major to the minor axis should equal 2. For a sphere, this ratio should equal 1. The ratios for major to minor axes were determined for end-diastole and end-systole.

The end-diastolic radius (R)/wall thickness (Th) ratio was calculated as an estimate of end-diastolic volume/mass using the formula (17):

$$R/Th = (\text{Short axis area}/3.14)^{1/2}/\text{Posterior wall thickness.}$$

Left ventricular end-systolic meridional wall stress was calculated using the following formula (18):

$$\text{End-systolic stress} = 1.35(\text{ESP})(\text{ESD})/4(\text{ESPWT})\,(1 + \text{ESPWT}/\text{ESD}),$$

where ESP = aortic end-systolic pressure, ESD = M-mode left ventricular end-systolic dimension and ESPWT = end-systolic posterior wall thickness. These measures were calculated from three consecutive beats at each atrially paced stage.

Histology. Tissue specimens for microscopic examinations were taken from above and below the papillary muscle level, mid-papillary muscle level, anterior wall, intraventricular septum and posterior wall. Apical samples were also obtained. All samples obtained included the epicardial and endocardial surfaces. Tissue samples were stained with

Table 1. Variables of Left Ventricular Size and Systolic Function After Coronary Embolization

	Baseline	Acute LV Dysfunction	LV Dysfunction at 8 Weeks
EDA (cm^2)	10.2 ± 1.4	13.5 ± 1.4*	15.1 ± 2.1*‡
ESA (cm^2)	4.4 ± 1.5	10.4 ± 1.3*	10.6 ± 1.8*
AEF (%)	57 ± 9	24 ± 6*	29 ± 6*‡
RV EDA (cm^2)	5.6 ± 1.7	5.2 ± 1.7	5.6 ± 1.8
RV ESA (cm^2)	3 ± 1.2	2.8 ± 1.6	3.3 ± 1.9
RV AEF (cm^2)	46 ± 13	43 ± 12	41 ± 13
Peak +dP/dt (mm Hg/s)	2,087 ± 364	1,607 ± 243*	1,556 ± 361*
LVSP (mm Hg)	110 ± 13	101 ± 12†	112 ± 14‡
SV (cc/beat)	42 ± 6	23 ± 10*	32 ± 9*‡
MAP (mm Hg)	96 ± 8	91 ± 5†	97 ± 10
ESS (g/cm^2)	37 ± 7	89 ± 16*	88 ± 15*

*$p < 0.01$ (vs. baseline); †$p < 0.05$; ‡$p < 0.05$ (left ventricular [LV] dysfunction at 8 weeks vs. acute dysfunction). AEF = area ejection fraction; EDA = end-diastolic area; ESA = end-systolic area; ESS = end-systolic stress; LVSP = peak left ventricular systolic pressure; MAP = mean arterial pressure; Peak +dP/dt = peak positive first derivative of left ventricular pressure; RV = right ventricular; SV = stroke volume.

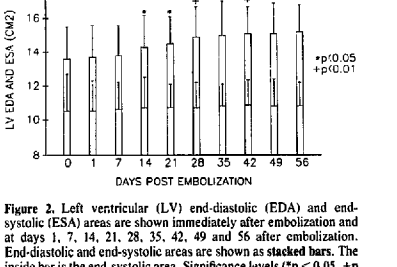

Figure 2. Left ventricular (LV) end-diastolic (EDA) and end-systolic (ESA) areas are shown immediately after embolization and at days 1, 7, 14, 21, 28, 35, 42, 49 and 56 after embolization. End-diastolic and end-systolic areas are shown as **stacked bars**. The inside bar is the end-systolic area. Significance levels (*$p < 0.05$, +$p < 0.01$) are based on comparisons versus baseline.

hematoxylin-eosin and Masson trichrome stains (to demonstrate collagen). Semiquantitative analysis of the extent of fibrosis was performed by determining the percent of a given low power field occupied by fibrosis (trichrome staining). Color slides were made from each glass slide and were projected on a white screen. Trichrome stained areas were outlined and measured by planimetry. For a particular wall and level, the extent of fibrosis was determined from the average of 18 low power fields (40×): three slides with three endocardial (inner half) and three epicardial (outer half) fields per slide.

Statistics. Data are expressed as mean values ± SD and analyzed by analysis of variance with repeated measures of variance. If a p value < 0.05 was found for the F ratio, Tukey's test was used to determine whether significant ($p < 0.05$) differences existed for a given variable between any of the experimental conditions. The relation between two variables was determined by using least squares linear regression. A p value < 0.05 was considered significant.

Results

Left ventricular size and function and hemodynamics after coronary embolization (Table 1). Coronary artery microsphere embolization had a profound immediate influence on left ventricular systolic function, as characterized by an increase in left ventricular size at end-diastole and systole and end-systolic wall stress and a reduction in area ejection fraction, peak positive dP/dt, left ventricular systolic pressure, stroke volume and mean arterial pressure. At 8 weeks there was a compensatory further increase in left ventricular size associated with an improvement in stroke volume and area ejection fraction (Fig. 2). No changes were noted in end-systolic area. However, 14 days after embolization the left ventricular end-diastolic area increased and further increased at 28 days, after which time no further changes were noted. Left ventricular end-systolic area, peak positive dP/dt and end-systolic wall stress remained unchanged at 8 weeks. Left ventricular systolic pressure and mean arterial pressure at 8 weeks were similar to baseline measurements. Right ventricular size and systolic function did not change with acute left ventricular dysfunction. There was an insignificant decrease in right ventricular systolic function ($p = 0.10$) at 8 weeks primarily due to a small increase in end-systolic area.

Heart weight and mass and wall motion. Canine weight increased from 21.8 ± 3.2 kg before embolization to 23.7 ± 3.3 kg at 8 weeks ($p < 0.05$). There was no evidence of ascites or overt pulmonary congestion in any dog. Heart weight (mean) at 8 weeks was 188 ± 24 g or 7.92 ± 0.92 g/kg body weight. Heart weight was for obvious reasons not available after the induction of acute left ventricular dysfunction, however, earlier studies in our laboratory in eight dogs demonstrated a heart weight of 6.1 ± 0.9 g/kg body weight, which was significantly less ($p < 0.01$) than that of dogs studied 8 weeks after embolization. Septal and posterior wall thickness demonstrated insignificant increases at 8 weeks (septum 0.74 ± 0.07 cm at 8 weeks vs. 0.78 ± 0.16 cm before embolization; posterior wall 0.75 ± 0.06 cm vs. 0.78 ± 0.12 cm, p = NS). In contrast, acute left ventricular dysfunction resulted in mild wall thinning (septum 0.67 ± 0.11 cm, $p < 0.05$; posterior wall 0.66 ± 0.13 cm, $p < 0.05$). However, left ventricular mass increased significantly at 8 weeks (117 ± 24 vs. 92.2 ± 9 g, $p < 0.01$) as compared with baseline and after acute left ventricular dysfunction (94.2 ± 9.3 g, $p < 0.05$). Left ventricular systolic wall motion immediately after embolization and at 8 weeks demonstrated only global systolic impairment in all dogs as determined by semiquantitative visual assessment of wall motion.

Table 2. Left Ventricular Geometry After Coronary Embolization

	Baseline	Acute LV Dysfunction	LV Dysfunction at 8 Weeks
Major axis (cm)			
ED	5.41 ± 0.51	5.83 ± 0.82*	6.32 ± 0.71*‡
ES	4.22 ± 0.72	4.64 ± 0.62*	4.71 ± 0.53†
A4C minor axis (cm)			
ED	3.62 ± 0.41	4.74 ± 0.52*	5.14 ± 0.43*‡
ES	2.41 ± 0.41	4.24 ± 0.82*	4.23 ± 0.61*
Short-axis/minor axis (cm)			
ED	3.41 ± 0.32	4.64 ± 0.42*	5.04 ± 0.51*‡
ES	2.52 ± 0.31	4.13 ± 0.41*	4.23 ± 0.52*
Major axis/minor axis (A4C)			
ED	1.61 ± 0.42	1.18 ± 0.42*	1.38 ± 0.31*‡
ES	1.71 ± 0.43	1.11 ± 0.42*	1.13 ± 0.33*
Major axis/minor axis (short axis)			
ED	1.62 ± 0.51	1.16 ± 0.32*	1.37 ± 0.32*‡
ES	1.71 ± 0.42	1.12 ± 0.41*	1.11 ± 0.43*
R/Th			
ED	1.62 ± 0.41	2.83 ± 0.62*	2.40* ± 0.61*‡

*p < 0.01 (vs. baseline); †p < 0.05; ‡p < 0.05 (acute left ventricular [LV] dysfunction vs. dysfunction at 8 weeks). A4C = apical four-chamber; ED = end-diastole; ES = end-systole; R/Th = end-diastole radius/posterior wall thickness.

Left ventricular geometry (Table 2). With acute left ventricular dysfunction, there was an increase in the major and both minor axes at end-diastole and end-systole. The ratio of major to both minor axes demonstrated a more spheric left ventricle (smaller ratio) with acute left ventricular dysfunction. The left ventricular radius/wall thickness ratio increased. At 8 weeks after the induction of left ventricular dysfunction, the major and both minor axes further increased at end-diastole only as compared with values during acute left ventricular dysfunction. The left ventricle became less spheric at end-diastole and the left ventricular radius/wall thickness ratio at end-diastole decreased as compared with the value during acute left ventricular dysfunction.

Diastolic timing intervals (Table 3). With acute left ventricular dysfunction, the timing of the onset of mitral filling was delayed and was associated with prolongation of the isovolumetric relaxation period and shortening of the diastolic and rapid filling periods. At 8 weeks there were shortening of the isovolumetric relaxation period, although it was still prolonged, normalization of the rapid filling period and shortening of the atrial filling period and pressure half-time.

Table 3. Diastolic Timing Intervals

	Baseline	Acute LV Dysfunction	LV Dysfunction at 8 Weeks
RR (ms)	702 ± 125	702 ± 125	702 ± 125
QMVO (ms)	258 ± 84	346 ± 36*	337 ± 41*
IRP (ms)	28 ± 9	66 ± 22*	45 ± 16*‡
DFP (ms)	344 ± 38	267 ± 75*	276 ± 62*
RFP (ms)	182 ± 48	164 ± 38†	181 ± 34†
AFP (ms)	93 ± 22	104 ± 26	84 ± 21†
P1/2T (ms)	57 ± 21	62 ± 18	36 ± 16‡

*p < 0.01 (vs. baseline); †p < 0.05; ‡p < 0.01 (acute left ventricular [LV] dysfunction vs. dysfunction at 8 weeks). AFP = atrial filling period; DFP = diastolic filling period; IRP = isovolumetric relaxation period; P1/2T = pressure half-time; QMVO = Q wave to onset of mitral flow; RFP = rapid filling period; RR = RR interval.

Hemodynamic variables of diastolic dysfunction (Table 4). Acute left ventricular dysfunction resulted in increased left ventricular end-diastolic and minimal pressures and mean right atrial pressure, which demonstrated further increases at 8 weeks. Peak negative dP/dt decreased and the time constant of relaxation increased with acute left ventricular dysfunction and remained unchanged at 8 weeks. The rapid filling wave on the left ventricular pressure tracing significantly increased at 8 weeks as compared with that at baseline and during acute left ventricular dysfunction. The chamber stiffness constant increased immediately after embolization and further increased at 8 weeks.

The filling fractions (Fig. 3 and Table 5) at one third and one half of diastole decreased with acute moderate left ventricular dysfunction, as previously noted in our laboratory (5). However, at 8 weeks after the induction of left ventricular dysfunction, both filling fractions increased to levels higher than those measured at baseline. We previously

Table 4. Hemodynamic Variables of Diastolic Function

	Baseline	Acute LV Dysfunction	LV Dysfunction at 8 Weeks
LVminP (mm Hg)	3 ± 2	6 ± 3*	6 ± 2*
LVEDP (mm Hg)	6 ± 2	13 ± 4*	17 ± 4*
Peak −dP/dt (mm Hg/s)	−1,680 ± 395	−1,148 ± 170*	−1,228 ± 363*
T (ms)	29 ± 7	46 ± 12*	50 ± 9*
RFW (mm Hg)	3 ± 1	3 ± 2	7 ± 4*
RAP (mm Hg)	3 ± 2	6 ± 3†	11 ± 4*‡
K	0.31 ± 0.18	0.48 ± 17*	0.58 ± 0.16*

*p < 0.01 (vs. baseline); †p < 0.05; ‡p < 0.01 (acute left ventricular [LV] dysfunction vs. dysfunction at 8 weeks). K = chamber stiffness constant; LVEDP = left ventricular end-diastolic pressure; LVminP = left ventricular minimal pressure; Peak −dP/dt = peak negative first derivative of left ventricular pressure; RAP = mean right atrial pressure; RFW = rapid filling wave; T = time constant of left ventricular pressure decline.

JACC Vol. 18, No. 7
December 1991:1794–803

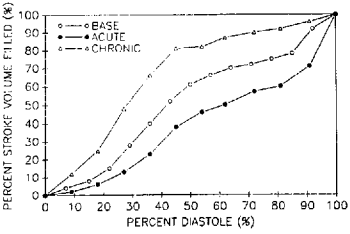

Figure 3. Percent stroke volume filled is plotted against the percent of diastole at baseline (BASE), after acute left ventricular dysfunction (ACUTE) and after 8 weeks (CHRONIC) for a representative dog. Impaired early diastolic filling is noted for acute left ventricular dysfunction and "supernormalization" of early diastolic filling is noted at 8 weeks after embolization.

observed (5) this phenomenon after induction of more severe acute left ventricular dysfunction associated with a severely elevated left ventricular end-diastolic pressure.

The peak rapid filling velocity, rapid filling fraction, peak rapid filling/peak atrial filling velocity ratio and rapid filling/atrial filling fraction ratio declined immediately after embolization, whereas the atrial filling fraction increased. Mitral regurgitation, as assessed by color flow mapping of the left atrium, was present in two dogs and occupied 9% and 12% of the left atrial area. At 8 weeks after embolization, there was redistribution of diastolic filling to early diastole, as characterized by increased peak rapid filling velocity, rapid filling fraction, the ratio of their peak velocities and filling fractions associated with a decrease in the rate and extent of atrial filling. The apparent normalization or supernormalization of diastolic filling variables was consistent with a "restrictive filling pattern" further corroborated by a shortened pressure half-time, an increased rapid filling wave and an increased chamber stiffness constant. Mitral regurgitation was present *in only three dogs* at 8 weeks with the regurgitant jet occupying 7%, 11% and 14% of the left atrial area, respectively.

Examination of the left ventricular diastolic pressure-area curve (Fig. 4) demonstrated a rightward shift with acute left ventricular dysfunction. A further rightward shift with a visibly greater slope of the ascending limb of the pressure-area curve was noted at 8 weeks correlating with a greater chamber stiffness constant as compared with that immediately after embolization.

Gross and histologic changes. Gross and histologic examination of each heart demonstrated the absence of scarring of the right ventricle and atria. There was diffuse, patchy scarring throughout the left ventricle. Histologic examination (Fig. 5) revealed microspheres in all layers of the left ventricle, usually single but occasionally multiple, in small

Table 5. Variables of Diastolic Filling

	Baseline	Acute LV Dysfunction	LV Dysfunction at 8 Weeks
FF-1/3 D (%)	44 ± 13	19 ± 10*	60 ± 17†‡
FF-1/2 D (%)	62 ± 14	39 ± 14*	83 ± 11†‡
E (cm/s)	75 ± 14	61 ± 12*	70 ± 10*
A (cm/s)	51 ± 19	50 ± 13	41 ± 12†
E/A	1.5 ± 0.5	1.2 ± 0.4†	1.9 ± 0.8*‡
RFF (%)	64 ± 9	55 ± 7*	71 ± 8*‡
AFF (%)	29 ± 11	45 ± 9*	24 ± 7‡
RFF/AFF	2.4 ± 0.9	1.5 ± 0.6*	3.1 ± 0.7*‡

*$p < 0.01$ (vs. baseline); †$p < 0.05$; ‡$p < 0.01$ (acute left ventricular [LV] dysfunction vs. dysfunction at 8 weeks). A = peak atrial filling velocity; AFF = atrial filling fraction; E = peak rapid filling velocity; FF-1/2 D = filling fraction at one-half diastole; FF-1/3 D = filling fraction at one-third diastole; RFF = rapid filling fraction.

arteries and arterioles surrounded by organized fibrotic scars in the interstitium (perivascular fibrosis), as well as replacing the myocardium (replacement fibrosis) with scattered intact myocytes. With use of a semiquantitative analysis, as characterized by the percent of trichrome staining in a given lower power field, no significant differences were noted in the location of a given wall or location (endocardial or epicardial) within the wall. The percent fibrosis ranged from 11% to 32%. We did not observe infarcts in various stages of healing, as has been previously described (8).

Discussion

Model of chronic left ventricular dysfunction. Recently several reports (2,3) have described a canine model of dilated congestive heart failure produced by rapid right ventricular pacing (rates >200 beats/min). Hemodynamic

Figure 4. Left ventricular (LV) pressure is plotted against left ventricular echocardiographic short-axis areas during diastole at baseline (BASE), after acute left ventricular dysfunction (ACUTE) and at 8 weeks after embolization (CHRONIC) for a representative dog. Pressure-area curves shifted rightward with acute left ventricular dysfunction. A rightward shift was noted at 8 weeks with an increased slope of the pressure-area curve suggesting a further increase in chamber stiffness.

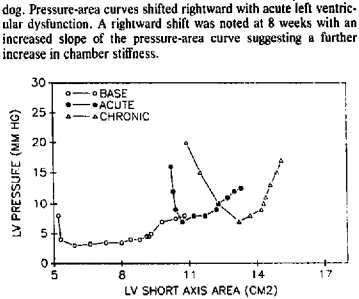

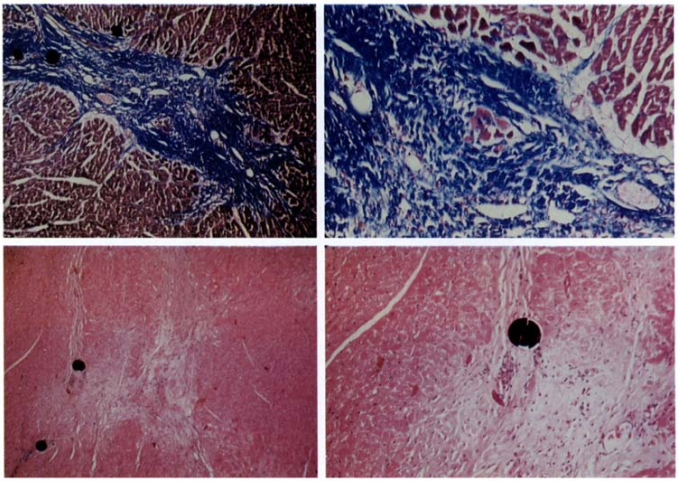

Figure 5. Photographs of a low power (×100) field (**left**) and high power field below (×200) (**right**). Hemotoxylin and eosin stains are **below** and Masson trichrome staining **above**. Patchy fibrosis begins interstitially and extends outward replacing the myocardium.

and neurohormonal data suggest that this model approximates nonischemic biventricular failure in humans. As a model of chronic left ventricular dysfunction, it lacks histologic alterations, results in thinning of the myocardium, is associated with nonphysiologic heart rates and is often reversible when pacing is discontinued. Evidence of histologic alterations characterized by interstitial and myocardial fibrosis has been demonstrated to be common in congestive cardiomyopathy of several etiologies including coronary, viral and idiopathic disease (9). Because ischemia is a potent cause of necrosis acutely and fibrosis chronically, we utilized a model of diffuse ischemia produced by coronary artery microsphere embolization to produce a model of chronic left ventricular dysfunction with fibrotic scarring.

As in our previous observations (5), coronary microsphere embolization produced acute left ventricular systolic dysfunction characterized by increased left ventricular volumes, increased left ventricular end-diastolic and mean right atrial pressures, reduced stroke volume, reduced left ventricular area ejection fraction, reduced peak positive dP/dt and a more spheric left ventricle. Eight weeks after the induction of left ventricular dysfunction, left ventricular end-diastolic area increased further without a change in the end-systolic area, with a mild improvement in the area ejection fraction. Although left ventricular wall thickness was unaltered, left ventricular mass was increased. The left ventricle became less spheric at end-diastole. Left ventricular end-diastolic pressure and mean right atrial pressure further increased. The gross and histologic appearance of the left ventricle demonstrated patchy, diffuse scarring and focal myocardial fibrosis surrounding the site of microsphere occlusion.

The present study clearly indicates that acute left ventricular dysfunction induced by coronary microembolization can be developed into a model of chronic left ventricular dysfunction with elevated left ventricular filling pressures. This model demonstrates healing of acute microinfarctions and remodeling of the left ventricle, as demonstrated by increased cardiac weight, increased left ventricular volume and mass and a spheric shape, as compared with baseline findings. This model differs significantly from the rapid right ventricular pacing model in several respects. 1) It does not exhibit complete reversibility, although compensatory improvement in left ventricular systolic function and remodeling changes were noted. 2) Increased wall stress due to acute left ventricular dilation may have served as a stimulus to hypertrophy, minimizing the degree of wall thinning. In fact, left ventricular mass and cardiac weight increased. 3) Significant gross and histologic fibrosis were noted in our model,

although only minimal changes were noted in the gross or histologic appearance of the myocardium in the right ventricular pacing model. 4) Right ventricular dysfunction was noted in the pacing model, but only insignificant reductions in right ventricular systolic function were observed in our study.

Similarity of the model to clinical cardiomyopathy. Support for this model as a clinically relevant model of global left ventricular dysfunction can be gathered from the similarity of the myocardial histologic features found in this model and in idiopathic, coronary, viral and diabetic causes of cardiomyopathy (9,19). Furthermore, evidence exists supporting a role for microvascular ischemic and infarction as an etiologic factor for perivascular and replacement fibrosis: 1) The microscopic lesions seen in Syrian hampsters with cardiomyopathy are very similar to lesions seen in this model. Verapamil (calcium channel blocker) therapy may attenuate microvascular ischemia and slow the time course of cardiomyopathy (20). 2) Verapamil has also been shown to prevent the interstitial and replacement fibrosis seen in diabetic (streptozotocin) rats despite hyperglycemia (21). 3) Patients with dilated cardiomyopathy and angina have been shown to have impaired coronary vascular reserve, perhaps due to increased microvascular tone (22).

Finally, microembolization of the dog coronary tree with nonocclusive microspheres (25 μm) resulted in necrosis distal to the site of deposition despite perfusion beyond the site of microsphere deposition. Both verapamil and alpha$_1$-blockers prevented necrosis, suggesting that microvascular spasm may play a role (23).

Abnormalities of diastolic function in this model. Acute ischemic left ventricular dysfunction resulted in abnormalities of relaxation, delayed mitral valve opening, shortening of the diastolic filling period as a function of cycle length and a reduced rate and extent of early diastolic filling with an increased rate and extent of atrial diastolic filling. Reduced early diastolic filling has been previously demonstrated in acute (24,25) and chronic coronary artery disease (25), hypertension (26) and left ventricular hypertrophy (27,28). However, at 8 weeks a different diastolic filling pattern emerged, characterized by early redistribution of diastolic filling despite continued abnormal relaxation. The filling pattern was associated with a significant increase in the rapid filling wave, a further increase in left ventricular end-diastolic size and pressure and an increase in mean right atrial pressure. In the present study, diffuse, patchy fibrotic alterations suggested the possibility of a myocardial restrictive process, as characterized by an increase in the rapid filling wave of the left ventricular pressure tracing (29) and an increase in the chamber stiffness constant. In our previous acute studies (5), we found no evidence of increases in the rapid filling wave associated with marked increases in left ventricular filling pressure. However, it may be difficult to differentiate the individual influences of myocardial restraint and pericardial constraint. Similar patterns of diastolic filling have been noted in both restrictive myocardial processes and constrictive pericarditis (29,30). Similar alterations of the diastolic filling pattern have been noted in acute experimental heart failure and with hemodynamic maneuvers designed to increase pericardial restraint (volume loading) (5). However, in this study pericardial restraint cannot be invoked as a causative mechanism for the observed pattern of left ventricular diastolic filling for two reasons: 1) The pressure-area curves did not display upward displacements with chronic dysfunction. 2) We did not remove the pericardium to assess the influence on the left ventricular pressure-area relations and the diastolic filling pattern.

Limitations. The microsphere model that we have described results in only moderate left ventricular systolic dysfunction with significant elevation of left ventricular filling pressure. Although this model demonstrates global systolic dysfunction analogous to that seen in human cardiomyopathy, it does not completely reflect the heterogeneity of the diastolic filling patterns noted in patients with congestive cardiomyopathy, which may vary from impairment to enhancement of early diastolic filling (31,32). Because many of our study dogs exhibited a third heart sound, the observed diastolic filling pattern may be appropriate as it is commonly seen in patients with a third heart sound due to congestive cardiomyopathy (31,32). Because this model was only extensively studied at 8 weeks after embolization, it is possible that further remodeling, hemodynamic improvement or decompensation may occur with longer periods of observation.

Second, despite the histologic finding of fibrosis, we cannot be certain that the enhanced early diastolic filling pattern noted is the result of myocardial restriction. Fibrosis is common in patients with congestive cardiomyopathy, yet marked heterogeneity in filling patterns has been noted, probably related to the interrelations of the left atrial pressure at mitral valve opening, relaxation abnormalities, the presence of mitral regurgitation and pericardial constraining properties. Although early redistribution of diastolic filling at 8 weeks may be due to the influence of mitral regurgitation (33), mitral regurgitation was present in only three dogs.

The use of frame by frame assessment of two-dimensional echocardiographic left ventricular short-axis areas at the mid-papillary level as a method to assess diastolic filling has certain limitations relating to the inclusion of the isovolumetric relaxation period and to the frame rate. Because heart rates were <100 beats/min, at least 23 frames were available to analyze for a full cardiac cycle and 12 frames for diastole in all dogs. Because the differences in the isovolumetric relaxation period between acute and chronic left ventricular dysfunction were no greater than one video frame (>33 ms), it is unlikely that the frame by frame method obscured changes in the diastolic filling pattern because alterations in the filling fraction were profound. Similar but less profound alterations were noted with the Doppler transmitral spectral readings.

Conclusions. Coronary microsphere embolization-induced ischemic damage to the left ventricle resulted in a model of chronic moderate left ventricular systolic dysfunction asso-

ciated with prominent diastolic dysfunction characterized by a restrictive pattern of left ventricular diastolic filling.

References

1. Smith, NA. Experimental model of heart failure. Cardiovasc Res 1985; 19:181–6.
2. Wilson JR, Douglas P, Hickey WF, et al. Experimental congestive heart failure produced by rapid ventricular pacing in the dog: cardiac effects. Circulation 1987;75:857–67.
3. Armstrong PW, Stopps TP, Ford SE, DeBold AJ. Rapid ventricular pacing in the dog: pathophysiologic studies of heart failure. Circulation 1986;74:1075–84.
4. Smiseth OA, Mjos OD. A reproducible and stable model of acute ischemic left ventricular failure in dogs. Clin Physiol 1982;2:225–39.
5. Lavine SJ, Campbell CA, Kloner RA, Gunther SJ. Diastolic filling in acute left ventricular dysfunction: role of pericardium. J Am Coll Cardiol 1988;12:1326–33.
6. Lavine SJ, Campbell CA, Held AC, Johnson V. Effect of nitroglycerine-induced reduction of left ventricular filling pressure on diastolic filling in acute dilated heart failure. J Am Coll Cardiol 1989;14:233–41.
7. Lavine SJ, Krishnaswami V, Shreiner DP. Left ventricular diastolic filling pattern in patients with left ventricular dysfunction. Int J Cardiol 1985;8: 423–36.
8. Smiseth OA, Lindal S. Progression of myocardial damage following coronary microembolization in dogs. Acta Pathol Microbiol Immunol Scand 1985;91A:115–24.
9. Unverferth DV, Baker PB, Suifi SE, et al. Extent of myocardial fibrosis and cellular hypertrophy in dilated cardiomyopathy. Am J Cardiol 1986; 57:816–20.
10. Hamby RI, Zonaraich S, Sherman L. Diabetic cardiomyopathy. JAMA 1974;30:595–602.
11. Weiss JL, Frederickson JW, Weisfeldt ML. Hemodynamic determinants of the time course of fall in canine left ventricular pressure. J Clin Invest 1976;58:751–60.
12. Sahn DJ, De Maria A, Kissio J, Weyman A. Recommendations regarding quantization in M-mode echocardiography: results of a survey of echocardiographic measurements. Circulation 1978;58:1072–83.
13. Devereaux R, Reichek N. Echocardiographic determination of left ventricular mass in man. Circulation 1977;55:613–18.
14. Gaasch WH, Levine HJ, Quinones MA, Alexander JK. Left ventricular compliance: mechanisms and clinical implications. Am J Cardiol 1976;38: 645–53.
15. Mirsky I. Assessment of passive elastic stiffness of cardiac muscle: mathematical concepts, physiologic and clinical considerations; directions of future research. Prog CV Dis 1976;18:277–306.
16. Dodge HT, Sandler H, Ballew DW, Lord JD Jr. The use of biplane angiocardiography for the measurement of left ventricular volume in man. Am Heart J 1960;60:762–76.
17. Gaasch WH, Carroll JD, Levine HJ, Criscitiello MG. Chronic aortic regurgitation: prognostic value of left ventricular end-systolic dimension and end-diastolic radius/thickness ratio. J Am Coll Cardiol 1983;1:775–82.
18. Grossman W, Braunwald E, Mann T, McLaurin LP, Green LH. Contractile state of the left ventricle in man as evaluated for the end-systolic pressure-volume relation. Circulation 1977;56:845–52.
19. Regan TJ, Ettinger PO, Khan MI, et al. Altered myocardial function and metabolism in chronic diabetes mellitus without ischemia. Circ Res 1974;35:222–37.
20. Factor SM, Minase T, Cho S, Dominitz R, Sonnenblick EH. Microvascular spasm in the cardiomyopathic Syrian hamster: a preventable cause of focal myocardial necroses. Circulation 1982;66:342–54.
21. Afzal N, Ganguly PK, Dhalla KS, Pierce GN, Singal PK, Dhalla NS. Beneficial effects of verpamil in diabetic cardiomyopathy. Diabetes 1988; 37:936–42.
22. Cannon RO, Cannion RE, Parrillo JE, et al. Dynamic limitation of coronary vasodilator reserve in patients with dilated cardiomyopathy and chest pain. J Am Coll Cardiol 1987;10:1190–200.
23. Eng C, Cho S, Factor S, Sonnenblick EH, Kirk ES. Myocardial microinfarcts produced by microsphere embolization: role of alpha adrenergic tonic influence on the coronary microcirculation. Circ Res 1984;54:74–82.
24. Labovitz AJ, Lewen MK, Kern M, VanCormael M, Deligonal U, Kennedy HL. Evaluation of left ventricular systolic and diastolic dysfunction during transient myocardial ischemia produced by angioplasty. J Am Coll Cardiol 1987;10:749–55.
25. Bonow RO, Bacharach SL, Green MV, et al. Impaired left ventricular diastolic filling in patients with coronary artery disease: assessment with radionuclide angiography. Circulation 1981;64:315–23.
26. Inouye I, Massie B, Loge D, et al. Abnormal left ventricular filling: an early finding in mild to moderate systemic hypertension. Am J Cardiol 1984;53:120–6.
27. Shahk MA, Lavine SJ. Effect of mitral regurgitation on diastolic filling with left ventricular hypertrophy. Am J Cardiol 1988;61:390–4.
28. Hamrath P, Mathey DG, Siegert R, Bleifeld W. Left ventricular relaxation and filling patterns in different forms of left ventricular hypertrophy: an echocardiographic study. Am J Cardiol 1980;45:15–23.
29. Appleton CP, Hatle LK, Popp RL. Demonstration of restrictive ventricular physiology by Doppler echocardiography. J Am Coll Cardiol 1988; 11:757–68.
30. Tyberg TH, Goodyear AVN, Hurst VW, Alexander J, Langou RA. Left ventricular filling in differentiating restrictive amyloid cardiomyopathy and constrictive pericarditis. Am J Cardiol 1981;47:791–6.
31. Lavine SJ, Arends D. Diastolic filling correlates of the S3. Am J Noninvasive Cardiol 1989;3:51–7.
32. Lavine SJ, Arends D. Importance of the left ventricular filling pressure on diastolic filling in idiopathic dilated cardiomyopathy. Am J Cardiol 1989;64:61–5.
33. Takenaka K, Dabestani A, Gardin JM, et al. Pulsed Doppler echocardiographic study of left ventricular filling in dilated cardiomyopathy. Am J Cardiol 1986;58:143–7.